Chemical Physics Letters 684 (2017) 117–125

Contents lists available at ScienceDirect

Chemical Physics Letters

journal homepage: www.elsevier.com/locate/cplett

Research paper

Size-dependent adsorption sites in a Prussian blue nanoparticle: A 3D-RISM study

Nirun Ruankaew [a,b], Norio Yoshida [b,*], Yoshihiro Watanabe [b], Haruyuki Nakano [b], Saree Phongphanphanee [a,c,*]

[a] Department of Materials Science, Faculty of Science, Kasetsart University, Bangkok, Thailand
[b] Department of Chemistry, Graduate School of Science, Kyushu University, Fukuoka, Japan
[c] Computational Biomodelling Laboratory for Agricultural Science and Technology, Faculty of Science, Kasetsart University, Bangkok, Thailand

ARTICLE INFO

Article history:
Received 22 March 2017
In final form 23 June 2017
Available online 24 June 2017

Keywords:
Prussian blue
Cesium
Selective adsorption
3D-RISM
Ion selectivity
Adsorption site

ABSTRACT

The specific adsorption of alkali ions, Li^+, Na^+, K^+, and Cs^+, in electrolyte solutions on Prussian blue (PB) is investigated by using the three-dimensional (3D) reference interaction site-model (RISM) theory. The results from 3D-RISM show dramatically different adsorption sites between large ions (K^+ and Cs^+) and small ions (Li^+ and Na^+). The small ions are adsorbed at the channel entrance sites without the water–ion exchange mechanism. In contrast, the large ions are adsorbed in PB by the water–ion exchange mechanism, and the adsorption site of large ions is located at the center of the cage or at the interstitial site.

1. Introduction

Prussian blue (PB) is a famous inorganic dye pigment of dark blue color, which was the first synthesized pigment. The German alchemist, Johann Jacob Diesbach, accidentally discovered it in the early 18th century [1]. PB, also known as ferric hexacyanoferrate(II), has a cubic framework and the chemical formula $Fe^{III}_4[Fe^{II}(CN)_6]_3{\cdot}xH_2O$. In its crystal, Fe^{3+} ions form a face-centered cubic with lattice constant (α) 10.166 Å, and Fe^{2+} ions are located at the midpoints of each side of the cube [2–5]. These two kinds of Fe are linked with cyanide groups in such a way that C atoms coordinate octahedrally with Fe^{2+}, and N atoms with Fe^{3+} (Fig. 1a). A defect in the crystal can arise from the vacancy of $[Fe^{II}(CN)_6]$ and can create a spherical cavity.[5,6] Fe ions in PB can be replaced by other bivalent or trivalent transition metal ions, such as Ni, Mn, Cu, Cd, Zn, and Co, the compounds of which are called PB analogue (PBA) compounds [7].

In the 200 years since its discovery, PB has been widely used in many fields of science, such as chemistry, pharmaceutics, medicine, nanomaterials, and various industrial applications [8,9]. PB and PBAs have fascinating properties, such as high adsorption and electrochemical long-cycle life performance, they have attracted much attention as materials for electrocatalysis, bio sensing, ion sensing, ion storage, and magnetism [9–16]. One of the most interesting abilities of PB is its excellent adsorption capacity and high selectivity to the specific alkali ion, especially the radioactive Cs [6]. For this reason, PB has been used as a removal antidote for poisoning by radioactive Cs and Tl; the usage of PB has been approved by the U.S. Food and Drug Administration (FDA) as a safe and effective treatment for internal radioactive contamination [1,13]. Recently, composites of PB and other nanomaterials, such as carbon nanotube (CNT) or graphene, have been considered for development of PB with enhanced properties [9,10].

Experiments show that the ionic selectivity depends on the size of the ions and that the selectivity sequence is $Cs^+ > K^+ > Na^+ > Li^+$ [17]. On the other hand, Cs^+ adsorption rate in PB is extremely slow; it takes approximately two weeks to complete the adsorption equilibrium at room temperature. This slow adsorption stems essentially from the large resistance of PB to intracrystalline diffusion. From the literature review, the intracrystalline diffusion coefficient is approximately at 3.3×10^{-22} m^2/s [18]. Moritomo and Tanaka reported that a change in pH and temperature can also affect the absorption rate of Cs^+ in PB [19]. The adsorption mechanism between PB and cations has been hypothesized as an

* Corresponding authors at: Department of Materials Science, Faculty of Science, Kasetsart University, Bangkok, Thailand (S. Phongphanphanee). Department of Chemistry, Graduate School of Science, Kyushu University, Fukuoka, Japan (N. Yoshida).

E-mail addresses: noriwo@chem.kyushu-univ.jp (N. Yoshida), fscisrph@ku.ac.th (S. Phongphanphanee).

http://dx.doi.org/10.1016/j.cplett.2017.06.053
0009-2614/

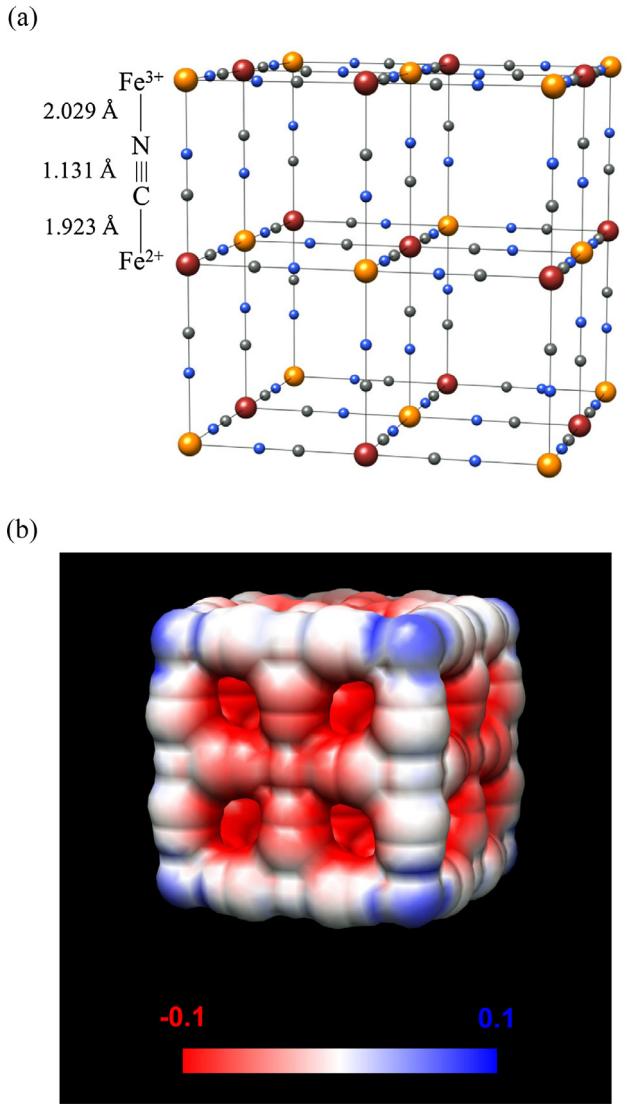

Fig. 1. (a) Unit lattice of PB ($Fe[Fe(CN)_6]_4{\cdot}xH_2O$). Brown spheres represent Fe^{2+} ions, and orange stands for Fe^{3+}, gray for C, and blue for N atoms [4]. (b) Electrostatic Potential Map of Prussian blue in atomic unit. (For interpretation of the references to colour in this figure legend, the reader is referred to the web version of this article.)

ion-exchange process [9,20]. Recently, Ishizaki et al. proposed that Cs^+ ions are adsorbed into PB interstitial sites by simple physical adsorption [6]. Furthermore, Moritomo and coauthors showed that the binding positions and alignment of alkali ions depend on the distortion of the PB lattice [21]. However, the basis for the ion selectivity and the intercalation mechanism between PB and alkali ions in equilibrium conditions are still unclear. The understanding of the ion selectivity in PB can be applied to designing new effective materials for removal of hazardous radioactive metal from contaminated water.

In this work, we examine the ion selectivity in PB by using the statistical mechanics theory of liquids called the 'three-dimensional (3D) reference interaction site model (RISM).'

Table 1
Lennard-Jones parameters of solute atom.

Atoms	σ (Å)	ε (J mol^{-1})
Fe	2.5943	54.3920
C	3.4309	439.320
N	3.2607	288.696

The theory is based on the site–site Ornstein–Zernike equation and can be used to determine the distribution of water and ions in PB. Various thermodynamic properties, such as solvation free energy or partial molar volume, can be also calculated from the distribution functions (DFs). The method has been successfully applied to many problems, such as solvation of biomolecules, organoclays, or nanoscale materials [22,23]. To understand how and where ion selectivity occurs, the 3D DFs of electrolyte solutions, LiCl, NaCl, KCl and CsCl, around and inside the PB single lattice were calculated by means of 3D-RISM. We also investigated the solvation structures around an alkali ion by applying the explicit ions at the most preferable position in PB.

2. Computational method

In 3D-RISM calculation, we considered a subunit of perfect crystal of PB—i.e., a no-defect crystal—as a solute immersed in

Table 2
Lennard-Jones parameters of solvent species.

Force Field	Atoms	q (e)	σ (Å)	ε (J mol^{-1})
SPC	O	−0.82	3.166	650.200
	H	+0.41	0.400	192.500
OPLS	Cl^-	−1.00	4.416	492.800
	Li^+	+1.00	2.127	76.479
	Na^+	+1.00	3.330	11.598
	K^+	+1.00	4.935	1.372
	Cs^+	+1.00	6.716	0.339

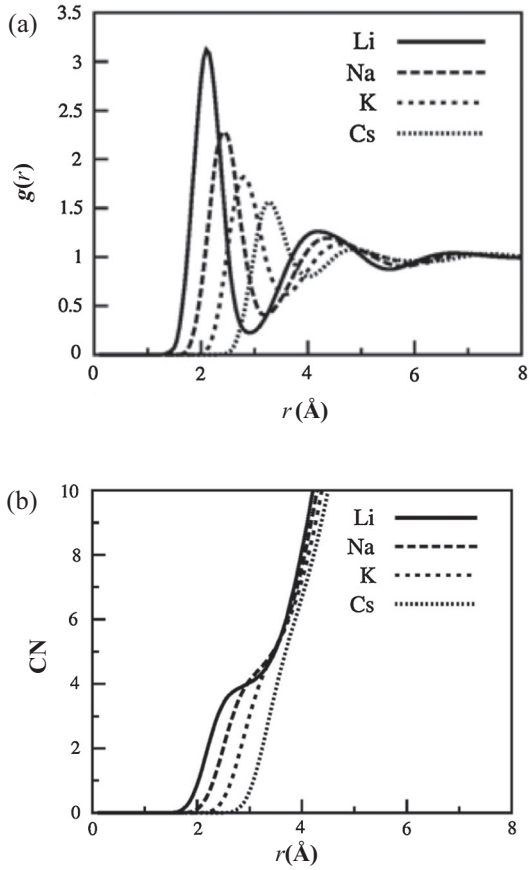

Fig. 2. (a) RDFs between oxygen site of water and all cation species in bulk water ($g(r)$) and (b) coordination number (cn) of water around the cations. r denotes the separation between the cation and solvent water oxygen.

electrolyte solutions at infinite dilution. The structure of the PB was taken from X-ray crystallography by Buser et al. The bond lengths between atoms in Fe^{2+}–C, Fe^{3+}–N, and C–N are 1.923, 2.029, and 1.131 Å, respectively [2]. For clarity, water molecules that were accompanied by the parent formula in the structure were removed because we aimed to focus only on the main skeleton of PB. To assign the partial charge on the solute sites, the electrostatic potential (ESP) charges were calculated by the Hartree–Fock method using Gaussian 09 Revision B. 01 [24]. The standard basis set, LANL2DZ, the effective core potential basis set, was used for the frozen inner core electrons up to the 2p orbital for all Fe atoms, and the 6-31G(d) basis set was applied for all C and N atoms [25–28]. The spin configuration of the mixed valence $Fe^{2+/3+}$ was omitted because the resultant energy difference between the high and low spin is not significant [29]. The Lennard-Jones (LJ) parameters of a PB particle were taken from the unified force field (UFF) [30,31] (see Table 1). For the solvents, SPC and OPLS parameters were used for water and ions [32] (Table 2) of aqueous solutions of LiCl, NaCl, KCl and CsCl at 0.1 M. We adopted 0.4 Å and 0.0460 kcal/mol for σ and ε of the LJ parameters of H of water, respectively [33,34]. This parameters set of solvents give a good agreement of the mean activity coefficient with the experimental results [23]. The temperature and dielectric constant in the calculations were 298 K and 78.5, respectively. The solvent–solvent correlation functions of the electrolyte solutions were obtained by dielectrically consistent RISM (DRISM) [35,36]. The number of grids in the calculations was 8192 and the width was 0.02 Å. The PB lattice was placed into the electrolyte solutions individually, and the 3D-RISM equation was solved in coupling with the Kovalenko–Hirata closure equation (KH closure) [37,38]. The condition parameters for 3D-RISM calculations were performed for 298 K and a dielectric constant of 78.5. The box size in all 3D-RISM calculations was $64 \times 64 \times 64$ Å^3 with a spacing of 0.5 Å, which created a $128 \times 128 \times 128$ grid. The potential parameters of explicit ions are same as the parameters used in implicit ion calculation. The numerical tolerance for DRISM and 3D-RISM were 1×10^8 and 1×10^6, respectively. For the Gaussian calculation, we employed SCF = TIGHT option for the iterative SCF calculations. For the explicit ions calculation, we used water as a solvent for investigating the solvation of ions in PB. Our DRISM and 3D-RISM calculations were performed by using an in-house software [39].

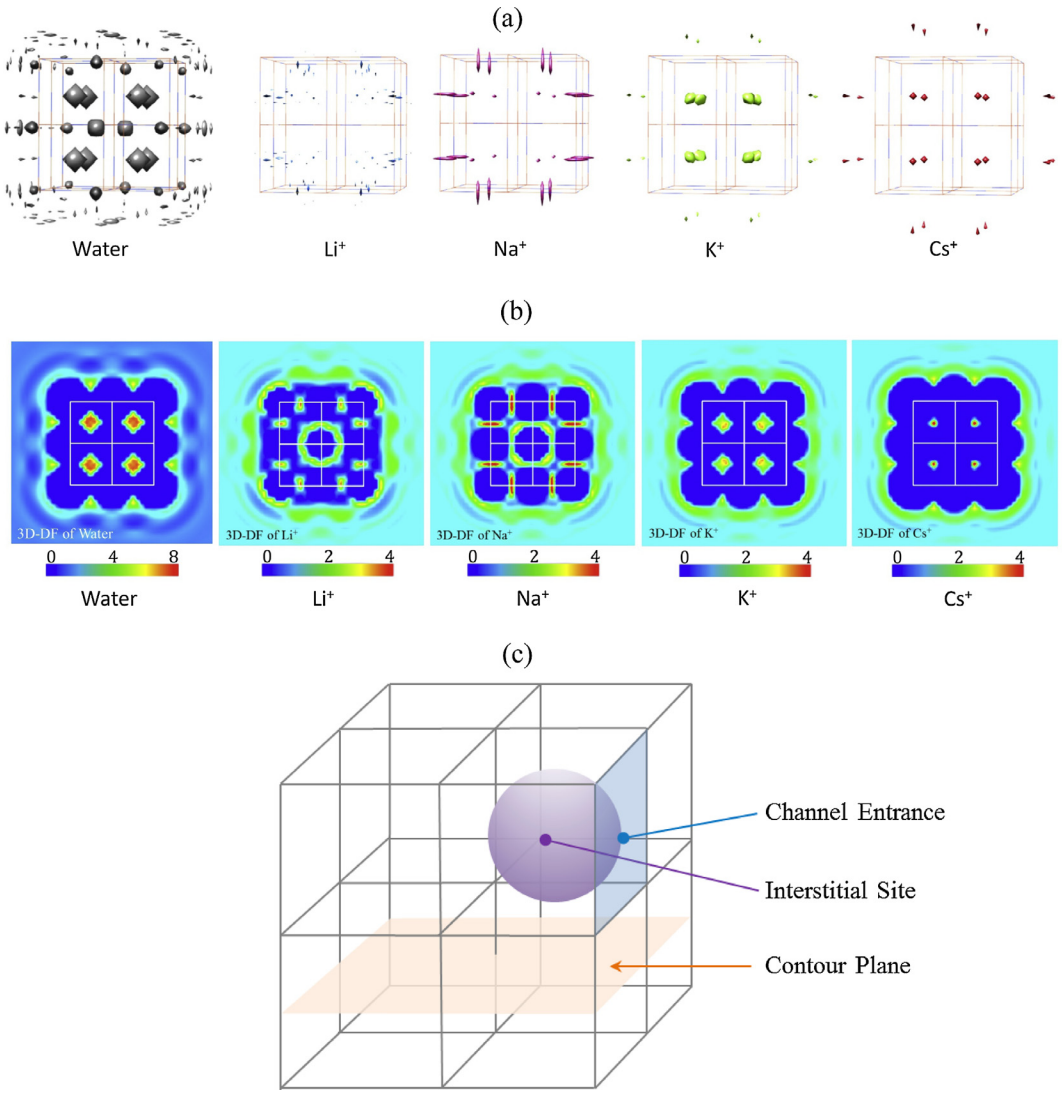

Fig. 3. (a) Isosurface plots of 3D-DFs of oxygen of water (gray), Li^+ (blue), Na^+ (purple), K^+ (green) and Cs^+ (red) when $g(r) > 3$, in and outside of PB; (b) the contour plot of 3D-DF of water and implicit ions, Li^+, Na^+, K^+, and Cs^+; and (c) illustration of terms of the PB site, where the channel entrance, interstitial site, and contour plane are defined. (For interpretation of the references to colour in this figure legend, the reader is referred to the web version of this article.)

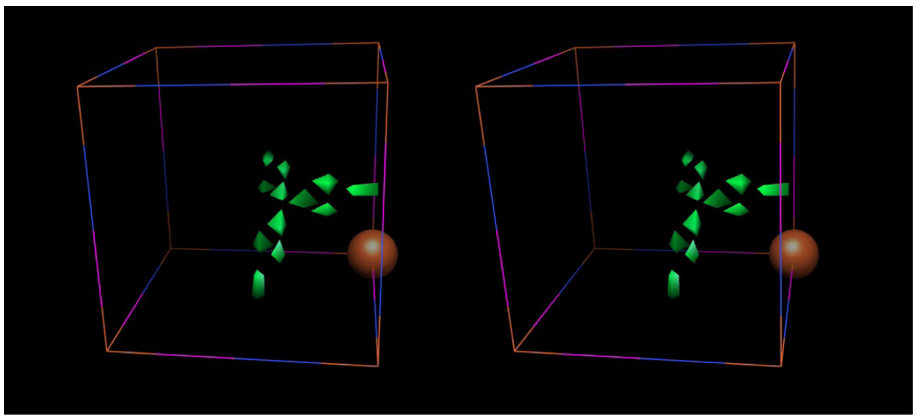

Fig. 4. The wall-eyed stereo view of 3D-DF of Li^+ inside the subcube of a unit cell of PB when $g_x(r)$ is greater than 2.5. The orange sphere represents the center Fe of the unit cell.

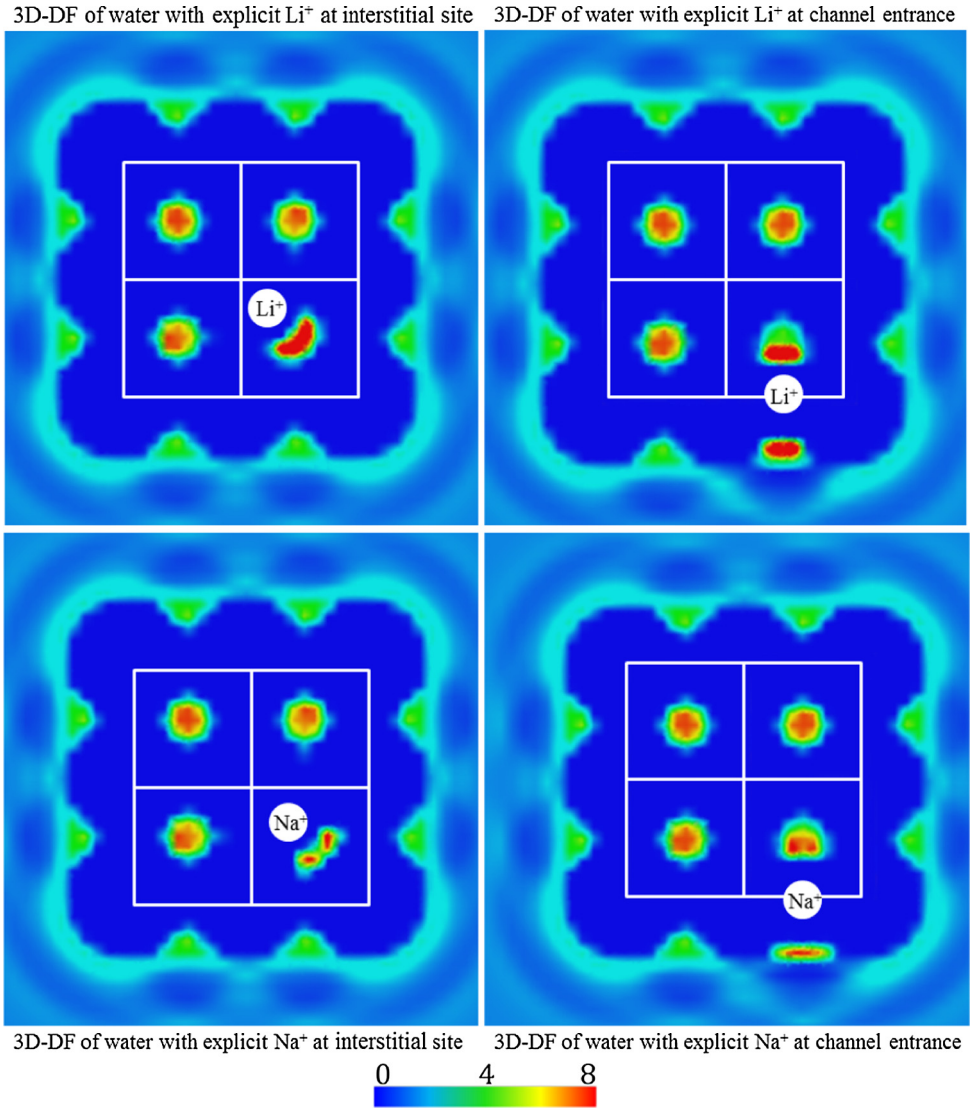

Fig. 5. (a) Contour plot of 3D-DF of water around PB (white cross-hatch square) and explicit Li^+ and Na^+ (white circle), (b) RDF of water-explicit Li^+ and Na^+ at the channel entrance and at the interstitial site, and (c) illustrate the water configuration of Li^+ at channel entrance of PB.

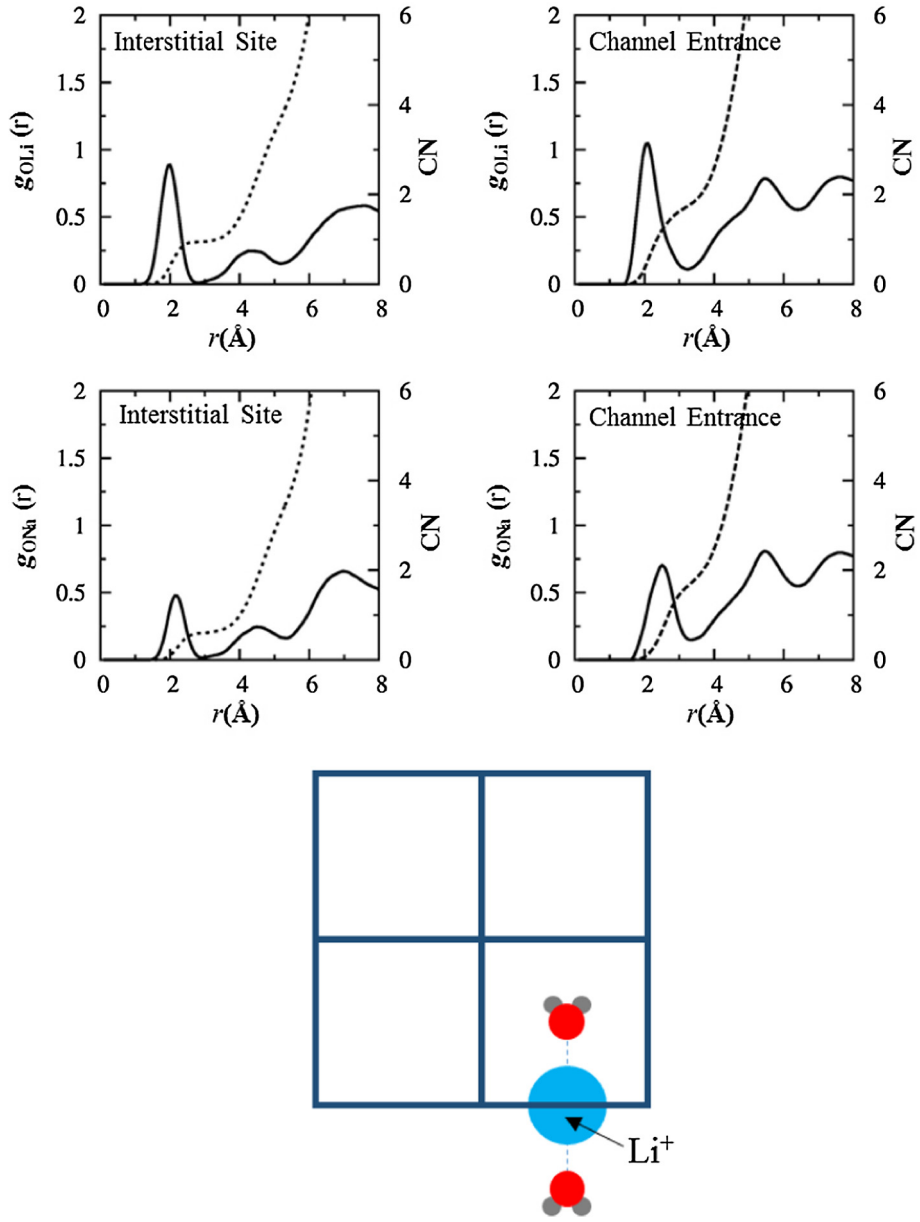

Fig. 5 (*continued*)

3. Results and discussion

3.1. Structure and bulk solutions

The electrostatic potential map of PB was computed by the Hartree–Fock method (Fig. 1b). Because of the π-backbonding between Fe^{2+} and six cyanide ligands at the center of the unit cell, the octahedral structure of $Fe^{2+}(CN)_6$ at the core-center of the PB produces a negative electrostatic environment. The negative potential might be the reason for the selectivity that PB shows for cations over anions. In contrast, the PB subunit produces a neutral and positively electrostatic potential on its surface and in the corner of the unit cell.

To investigate the ion selectivity of PB, we first performed 3D-RISM to obtain the solvation structure of ions in bulk water for the comparison of solvation of ions in bulk with those adsorbed by PB. The radial distribution functions (RDFs) of all cations (oxygen of water) are shown in Fig. 2a. The first maximum positions of the RDFs corresponding to the first solvation shell were at 2.1, 2.4, 2.9, and 3.3 Å for Li^+, Na^+, K^+, and Cs^+ respectively, which are in good agreement with previous experimental and simulation results [32,40]. The water coordination number (CN) of an ion was calculated by integrating the number of water density from the center of the ion to the first solvation shell,

$$CN = 4\pi\rho \int_0^b g(r) r^2 dr \quad (1)$$

where ρ and b are the water density and the radial distance of the first minimum, respectively. We found that in bulk water, Li^+, Na^+, K^+, and Cs^+ were coordinated by 3.91, 4.39, 5.12, and 6.68 water molecules, respectively, which fall in the range reported in the literature [41–43]. It is noted that the first solvation shell and the CN of the ions are in accordance with the ionic sizes.

3.2. Water and ions distribution around PB

Fig. 3a illustrate the 3D plots 3D-DF for the oxygen of water, Li^+, Na^+, K^+, and Cs^+ around and inside the PB. The 3D-DF of the solvent species x, $g_x(\mathbf{r}) > 3$ implies that the probability of finding solvent species x at position **r** is three times greater than that of bulk [44]. The contour maps for 3D-DFs of water and ions are given in Fig. 3b. The position of the contour plane is defined as the plane passing through the center of the subcube of a unit cell, and parallel to the surface (Fig. 3c). We also define in Fig. 3c the terms 'channel entrance' and 'interstitial site' for the following discussion. Water had the highest distribution peaks at the center of the interstitial sites, and other lower peaks appeared at the front of the channel entrance (Fig. 3a and b). The number of water molecules inside the PB lattice was calculated from the RDF of water centered at the center of the cube (Eq. (1)). We found that there were 7.4 water molecules distributed in the PB lattice, which means that a water molecule is bound in an interstitial site.

The 3D-DFs of Li^+ and Na^+ showed similar distribution patterns; their peaks appeared at an interstitial site and at the channel entrance (Fig. 3a and b). Furthermore, the highest peaks of these ions appeared at the channel entrance site, and this indicated that a small alkali ion, Li^+ or Na^+, was adsorbed at this position. At an interstitial site, the distribution peaks were not located at the center of the subcube. They were actually aligned on the diagonal planes (Fig. 4). The distance between the peaks of Li^+ and the central Fe^{3+} was closer than that of Na^+.

Similar to the distribution of water, the highest peak of 3D-DFs of K^+ and Cs^+ was located almost at the center of the subcube, and another peak appeared at the front of the channel entrance (Fig. 3b). Moreover, the front channel of the peak position of water, K^+, and Cs^+ do not coincide to each other's. Note that the binding positions of the smaller and larger ions were located at different sites. There was no DF peak of small ions at the front channel. These results indicate the different absorption mechanisms of large and small ions.

Ions intercalation into PB has been studied by density functional theory (DFT) and X-ray diffraction. The results of these methods were obtained without solvent environment [45,46]. In the DFT and experimental studies, the large ions, K^+ and Cs^+,

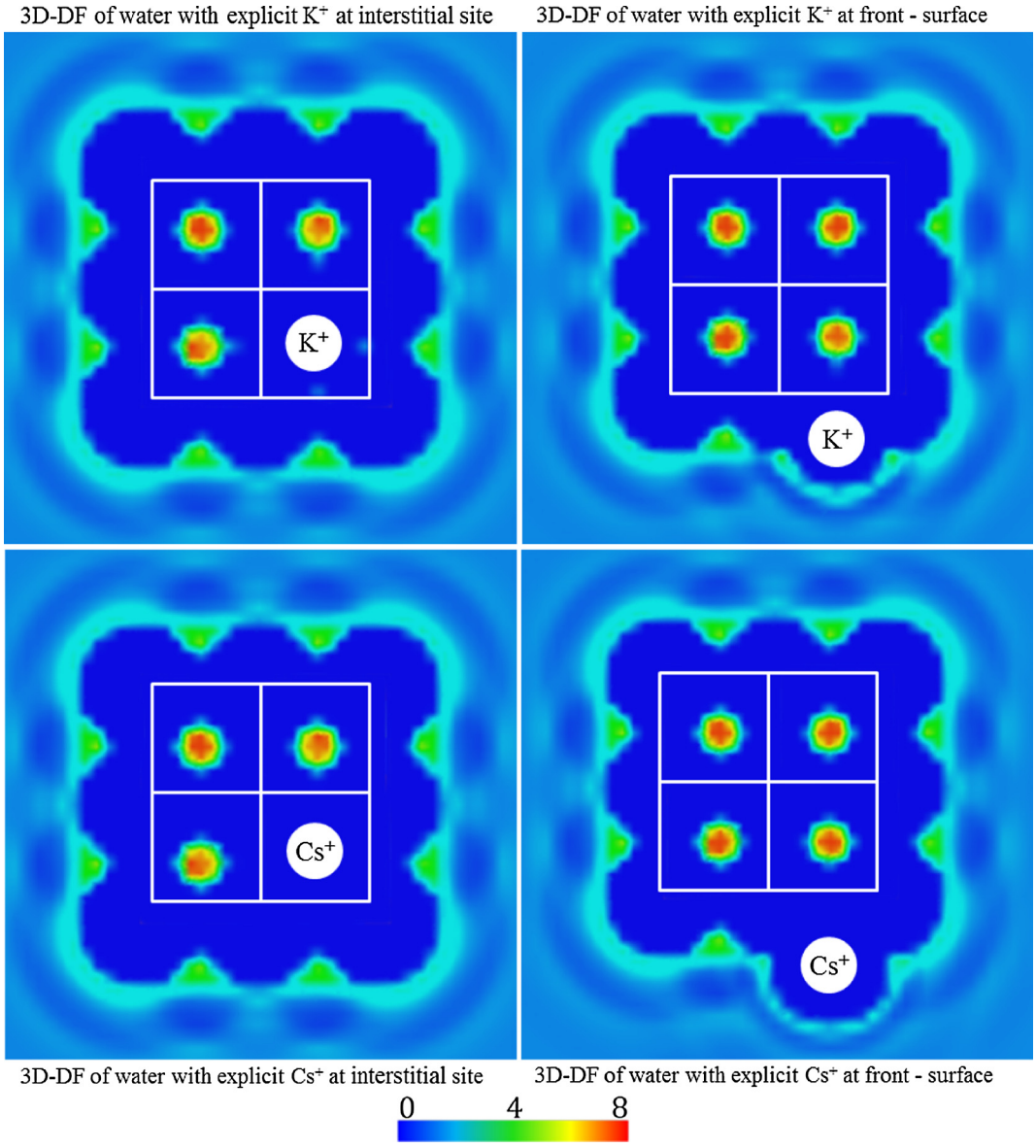

Fig. 6. (a) Contour plot of 3D-DF of water around PB (white cross-hatch square) and explicit K^+ and Cs^+, and (b) RDF of water-explicit K^+ and Cs^+ at the interstitial site and at the front surface, respectively.

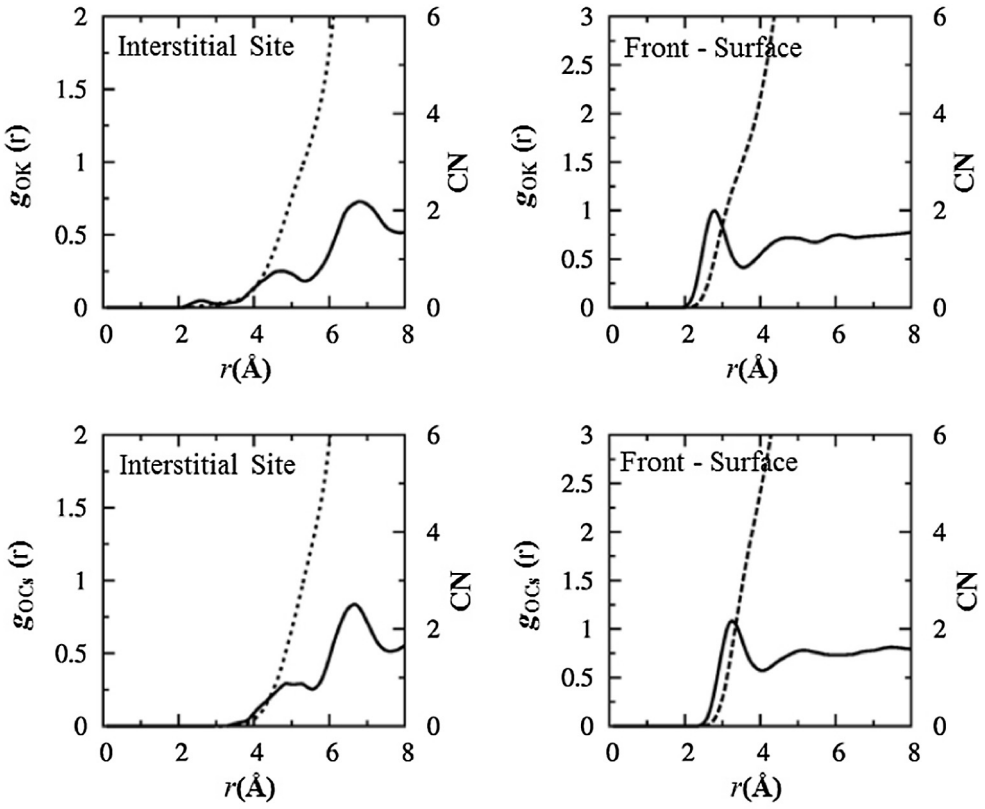

Fig. 6 (*continued*)

occupied the center of the interstitial sites, which is in good agreement with our results. For Na^+, the DFT study indicated that the ion is located at the face centers of subcube, which is consistent with the peak position of Na^+ at the entrance channel in our calculation. Furthermore, the X-ray diffraction results for $Na_{1:32}Mn[Fe(CN)_6]_{0:83}3{\cdot}6H_2O$ showed that the ion is located at an off-center position of the subcube, in the diagonal line between Fe and Mn. The peak positions of Na^+ in the interstitial site in our calculation were also at an off-center position and close to Fe at the center of the single unit cell (Fig. 3b). The position of Li^+ obtained from the DFT calculation was located at the site between the center of the subcube and the face center; however, our results indicated that the adsorption site of Li^+ is at the channel entrance or the face center of the subcube (Fig. 3a and b).

3.3. Explicit ions and intercalation mechanism

To elucidate the selective ion adsorption mechanism, we performed calculations with the PB and an explicit ion immersed in pure water. The 3D-DFs of the water molecules were calculated by placing the ion explicitly at the peak positions of its DF in the implicit model and examined the solvated structure of the explicit ion.

3.3.1. Solvated structure of explicit Li^+ and Na^+

To consider the water coordination of ions placed at the channel entrance or at an adsorption site, we calculated the 3D-DF of water in a system of PB with the explicit ion. The contour plot of the 3D-DF of water in the contour plane that was defined as Fig. 3c is shown in Fig. 5a. As can be observed, the explicit ions, Li^+ and Na^+, are coordinated by water in the interstitial site and at the front channel entrance. The RDF of water with respect to the explicit ion was calculated by angular averaging of the 3D-DF (Fig. 5b). The results show that the explicit ions, Li^+ and Na^+, were coordinated by almost two water molecules when the explicit ions were placed at the entrance channel. The number of water molecules in the PB cube was 7.3 for Li^+ and 7.0 for Na^+, whereas the number of water molecules in the PB cube without an explicit ion was 7.4. This means that the explicit ion is stabilized by one of the water molecules in the interstitial site and the other one in the front of the channel entrance (Fig. 5c). The complex of four cyanides and the ion, Li^+ or Na^+, is formed with two water molecules. This is similar to what we found in the case of Li^+ and water forming at the binding site of the selectivity filter of the K channel [44].

For the interstitial site, we placed the ions at the highest peak position of the 3D-DF for ions and performed the 3D-RISM calculation to evaluate the solvation structure. The *cn* of the explicit Li^+ and Na^+ placed at the interstitial site was 0.94 and 0.53, respectively. The results indicate that the ions in the site were partially dehydrated with only one water molecule remaining. This result is similar to the experimental studies of Rassat and Bácskai, who found that there is no ion and water exchange when the small ions, Li^+ or Na^+, are adsorbed and diffuse through the PB [20,47].

3.3.2. Solvated structure of explicit K^+ and Cs^+

As mentioned above, the adsorption sites of K^+ and Cs^+ were quite different from those of the smaller ions, Li^+ and Na^+. The adsorption site of the larger ions, K^+ and Cs^+, were located at the interstitial site, whereas those of the smaller ions were located at the channel entrance site. We placed an explicit ion, K^+ and Cs^+, at the front channel entrance site, which was the highest distribution position of the ion, and at the interstitial site, which is the adsorption site. The results of the 3D-DF and RDF of water around the explicit ions are shown in Fig. 6. When the explicit ions were placed at the interstitial site or the adsorption site, there was no water distribution at that site. This indicated that PB adsorbed

the fully dehydrated K^+ and Cs^+. The number of water molecules in the PB when K^+ or Cs^+ was adsorbed was 6.4. Then the water molecule at the interstitial site was removed when the adsorption ion occupied the site, which is consistent with the suggestion from the experiment with the water–ion exchange. Furthermore, Fig. 6 also shows the partially dehydrated structure of the explicit ions at the front channel entrance. The number of water molecules inside the PB that formed a complex with the explicit ion was 7.4 for both K^+ and Cs^+. Therefore, no water–ion exchange mechanism occurred in this state.

4. Conclusion

We have studied the adsorption of alkali ions on the PB unit cell using statistical mechanics of liquids called 3D-RISM. The results of 3D-DFs demonstrated that the large (K^+ and Cs^+) and small (Li^+ and Na^+) alkali ions are adsorbed at different sites through different mechanisms. The channel entrance is a specific binding site for the small ions, Li^+ and Na^+. At the adsorption site, two water molecules are bound to the small ion, where one water molecule is at the interstitial site and the other is at the front channel entrance. When the small ion penetrates into the PB, the water still stays inside the PB particle. There is no water–ion exchange during the adsorption or diffusion of small ions through PB. In contrast, the adsorbed large ions, K^+ and Cs^+, are bound to the center of the interstitial site with a fully dehydrated structure. For a large ion to adsorb into PB, one of the water molecules at the interstitial site must be removed. This result reinforces the experimental suggestion regarding the water–ion exchange mechanism of ion adsorption in PB.

In the present work, we have proposed the mechanism of the ion-size dependence on the ion-binding by PB. This mechanism is probably applicable also to the cage-size dependence on the ion binding by PB and PBA [39]. Therefore, we expect that the method used here will be useful for the high efficient ion-binding molecular design.

Acknowledgments

This work was financially supported by the Graduate School of Kasetsart University and the Kasetsart University Research and Development Institute (KURDI). We thank the International Affairs Division of Kasetsart University for providing the scholarship for our student. This work was also supported by Grants-in-Aid (25410021, 26104526, 16H00842, 16K05519, 26810008, 16H00778) from MEXT, Japan.

References

[1] H.A. Hoffman, L. Chakrabarti, M.F. Dumont, A.D. Sandler, R. Fernandes, Prussian blue nanoparticles for laser-induced photothermal therapy of tumors, Rsc Adv. 4 (2014) 29729–29734, http://dx.doi.org/10.1039/C4RA05209A.
[2] H.J. Buser, D. Schwarzenbach, W. Petter, A. Ludi, The crystal structure of Prussian Blue: Fe4[Fe(CN)6]3·xH2O, Inorg. Chem. 16 (1977) 2704–2710, http://dx.doi.org/10.1021/ic50177a008.
[3] J.F. Keggin, F.D. Miles, Structures and formulae of the Prussian blues and related compounds, Nature 137 (1936) 577–578, http://dx.doi.org/10.1038/137577a0.
[4] M.P. Shores, L.G. Beauvais, J.R. Long, Cluster-expanded Prussian blue analogues, J. Am. Chem. Soc. 121 (1999) 775–779, http://dx.doi.org/10.1021/ja983530s.
[5] V.K. Sharma, S. Mitra, N. Thakur, S.M. Yusuf, F. Juranyi, R. Mukhopadhyay, Dynamics of water in prussian blue analogues: neutron scattering study, J. Appl. Phys. 116 (2014), http://dx.doi.org/10.1063/1.4890722.
[6] M. Ishizaki, S. Akiba, A. Ohtani, Y. Hoshi, K. Ono, M. Matsuba, T. Togashi, K. Kananizuka, M. Sakamoto, A. Takahashi, T. Kawamoto, H. Tanaka, M. Watanabe, M. Arisaka, T. Nankawa, M. Kurihara, Proton-exchange mechanism of specific Cs+ adsorption via lattice defect sites of Prussian blue filled with coordination and crystallization water molecules, Dalt. Trans. 42 (2013) 16049, http://dx.doi.org/10.1039/c3dt51637g.
[7] P. Nie, L. Shen, H. Luo, B. Ding, G. Xu, J. Wang, X. Zhang, Prussian blue analogues: a new class of anode materials for lithium ion batteries, J. Mater. Chem. A. 2 (2014) 5852–5857, http://dx.doi.org/10.1039/c4ta00062e.
[8] A.A. Karyakin, Prussian blue and its analogues: electrochemistry and analytical applications, Electroanalysis 13 (2001) 813–819, http://dx.doi.org/10.1002/1521-4109(200106)13:10<813::AID-ELAN813>3.0.CO;2-Z.
[9] T. Vincent, C. Vincent, E. Guibal, Immobilization of metal hexacyanoferrate ion-exchangers for the synthesis of metal ion sorbents - a mini-review, Molecules 20 (2015) 20582–20613, http://dx.doi.org/10.3390/molecules201119718.
[10] X. Liu, G.R. Chen, D.J. Lee, T. Kawamoto, H. Tanaka, M.L. Chen, Y.K. Luo, Adsorption removal of cesium from drinking waters: a mini review on use of biosorbents and other adsorbents, Bioresour. Technol. 160 (2014) 142–149, http://dx.doi.org/10.1016/j.biortech.2014.01.012.
[11] A. Kumar, S.M. Yusuf, L. Keller, Structural and magnetic properties of Fe[Fe(CN)6]·4H_2O, Phys. Rev. B - Condens. Matter Mater. Phys. 71 (2005) 1–7, http://dx.doi.org/10.1103/PhysRevB.71.054414.
[12] S. Pintado, S. Goberna-Ferrón, E.C. Escudero-Adán, J.R. Galán-Mascarós, Fast and persistent electrocatalytic water oxidation by Co-Fe Prussian blue coordination polymers, J. Am. Chem. Soc. 135 (2013) 13270–13273, http://dx.doi.org/10.1021/ja406242y.
[13] N.L. Torad, M. Hu, M. Imura, M. Naito, Y. Yamauchi, Large Cs adsorption capability of nanostructured Prussian Blue particles with high accessible surface areas, J. Mater. Chem. 22 (2012) 18261, http://dx.doi.org/10.1039/c2jm32805d.
[14] C.D. Wessells, R.A. Huggins, Y. Cui, Copper hexacyanoferrate battery electrodes with long cycle life and high power, Nat. Commun. 2 (2011) 550–555, http://dx.doi.org/10.1038/ncomms1563.
[15] P. Xiao, J. Song, L. Wang, J.B. Goodenough, G. Henkelman, Theoretical study of the structural evolution of a Na 2 FeMn(CN) 6 cathode upon Na intercalation, Chem. Mater. 27 (2015) 3763–3768.
[16] C.D. Wessells, S.V. Peddada, M.T. McDowell, R.A. Huggins, Y. Cui, The effect of insertion species on nanostructured open framework hexacyanoferrate battery electrodes, J. Electrochem. Soc. 159 (2012) A98, http://dx.doi.org/10.1149/2.060202jes.
[17] L.F. Schneemeyer, S.E. Spengler, D.W. Murphy, Ion selectivity in nickel hexacyanoferrate films on electrode surfaces, Inorg. Chem. 24 (1985) 3044–3046, http://dx.doi.org/10.1021/ic00213a034.
[18] H. Fujita, H. Sasano, R. Miyajima, A. Sakoda, Adsorption equilibrium and kinetics of cesium onto insoluble Prussian blue synthesized by an immediate precipitation reaction between Fe3+ and [Fe(CN)6]4−, Adsorption 20 (2014) 905–915, http://dx.doi.org/10.1007/s10450-014-9635-7.
[19] Y. Moritomo, H. Tanaka, Alkali cation potential and functionality in the nanoporous prussian blue analogues, Adv. Condens. Matter Phys. 2013 (2013), http://dx.doi.org/10.1155/2013/539620.
[20] S.D. Rassat, J.H. Sukamto, R.J. Orth, M.A. Lilga, R.T. Hallen, Development of an electrically switched ion exchange process for selective ion separations, Sep. Purif. Technol. 15 (1999) 207–222, http://dx.doi.org/10.1016/S1383-5866(98)00102-6.
[21] T. Matsuda, J. Kim, Y. Moritomo, Control of the alkali cation alignment in Prussian blue framework, Dalt. Trans. 41 (2012) 7620, http://dx.doi.org/10.1039/c2dt12296k.
[22] J. Fafard, O. Lyubimova, S.R. Stoyanov, G.K. Dedzo, S. Gusarov, A. Kovalenko, C. Detellier, Adsorption of indole on kaolinite in nonaqueous media: organoclay preparation and characterization, and 3D-RISM-KH molecular theory of solvation investigation, J. Phys. Chem. C. 117 (2013) 18556–18566, http://dx.doi.org/10.1021/jp4064142.
[23] N. Yoshida, S. Phongphanphanee, F. Hirata, Selective ion binding by protein probed with the statistical mechanical integral equation theory, J. Phys. Chem. B. 111 (2007) 4588–4595.
[24] M.J. Frisch, G.W. Trucks, H.B. Schlegel, G.E. Scuseria, M.A. Robb, J.R. Cheeseman, G. Scalmani, V. Barone, B. Mennucci, G.A. Petersson, others, Gaussian 09, rev. B. 01, Gaussian Inc., Wallingford CT, 2010.
[25] M. Güell, J.M. Luis, M. Solà, M. Swart, Importance of the basis set for the spin-state energetics of iron complexes, J. Phys. Chem. A. 112 (2008) 6384–6391, http://dx.doi.org/10.1021/jp803441m.
[26] L.E. Roy, P.J. Hay, R.L. Martin, Revised basis sets for the LANL effective core potentials, J. Chem. Theory Comput. 4 (2008) 1029–1031, http://dx.doi.org/10.1021/ct8000409.
[27] Y. Yang, M.N. Weaver, K.M. Merz, Assessment of the '6–31+G** + LANL2DZ mixed basis set coupled with density functional theory methods and effective core potential: prediction of heats of formation and ionization potentials for first row transition metal complexes, J. Phys. Chem. A. 113 (2009) 9843–9851, http://dx.doi.org/10.1021/jp807643p.
[28] A. Ricca, C.W. Bauschlicher, A correlation-consistent basis set for Fe, Theor. Chem. Acc. 106 (2001) 314–318, http://dx.doi.org/10.1007/s002140100279.
[29] C. Daul, C. Rauzy, S. Decurtins, P. Franz, R. Hauser, DFT study of mixed-valent Mn(II/III) hexacyanide clusters, Int. J. Quantum Chem. 101 (2005) 753–760, http://dx.doi.org/10.1002/qua.20333.
[30] Q.M. Yu, W.A. Steen, K.M. Jeerage, S.Y. Jiang, D.T. Schwartz, Structure-dependent solvent and ion intercalation in reduced and oxidized nickel hexacyanoferrates, J. Electrochem. Soc. 149 (2002) E195–E203, http://dx.doi.org/10.1149/1.1474434.
[31] A.K.K. Rappé, C.J.J. Casewit, K.S.S. Colwell, W.A. Goddard III, W.M. Skiff, UFF, a full periodic table force field for molecular mechanics and molecular dynamics simulations, J. Am. Chem. Soc. 114 (1992) 10024–10035, http://dx.doi.org/10.1021/ja00051a040.

[32] K.P. Jensen, W.L. Jorgensen, Halide, ammonium, and alkali metal ion parameters for modeling aqueous solutions, J. Chem. Theory Comput. 2 (2006) 1499–1509, http://dx.doi.org/10.1021/ct600252r.
[33] B.M. Pettitt, P.J. Rossky, Integral equation predictions of liquid state structure for waterlike intermolecular potentials, J. Chem. Phys. 77 (1982) 1451–1457, http://dx.doi.org/10.1063/1.443972.
[34] K. Yoshida, T. Yamaguchi, A. Kovalenko, F. Hirata, Structure of tert-butyl alcohol−water mixtures studied by the RISM theory, J. Phys. Chem. B. 106 (2002) 5042–5049, http://dx.doi.org/10.1021/jp013400x.
[35] J.S. Perkyns, B. Montgomery Pettitt, A dielectrically consistent interaction site theory for solvent-electrolyte mixtures, Chem. Phys. Lett. 190 (1992) 626–630, http://dx.doi.org/10.1016/0009-2614(92)85201-K.
[36] J.S. Perkyns, B.M. Pettitt, A site-site theory for finite concentration saline solutions, J. Chem. Phys. 97 (1992) 7656–7666, http://dx.doi.org/10.1063/1.463485.
[37] A. Kovalenko, F. Hirata, Potential of mean force between two molecular ions in a polar molecular solvent: a study by the three-dimensional reference interaction site model, J. Phys. Chem. B. 103 (1999) 7942–7957, http://dx.doi.org/10.1021/jp991300+.
[38] A. Kovalenko, F. Hirata, Potentials of mean force of simple ions in ambient aqueous solution. I. Three-dimensional reference interaction site model approach, J. Chem. Phys. 112 (2000) 10391–10402, http://dx.doi.org/10.1063/1.481676.
[39] Y. Maruyama, N. Yoshida, H. Tadano, D. Takahashi, M. Sato, F. Hirata, Massively parallel implementation of 3D-RISM calculation with volumetric 3D-FFT, J. Comput. Chem. 35 (2014) 1347–1355, http://dx.doi.org/10.1002/jcc.23619.
[40] Y. Marcus, Ionic radii in aqueous solutions, J. Solution Chem. 12 (1983) 271–275, http://dx.doi.org/10.1007/BF00646201.
[41] I.G. Tironi, R. Sperb, P.E. Smith, W.F. van Gunsteren, A generalized reaction field method for molecular dynamics simulations, J. Chem. Phys. 102 (1995) 5451, http://dx.doi.org/10.1063/1.469273.
[42] Y. Tamura, H. Ohtaki, I. Okada, An MD simulation of concentrated aqueous solutions of caesium iodide, Zeitschrift Für Naturforsch. A. 46 (1991) 1083–1094, http://dx.doi.org/10.1515/zna-1991-1213.
[43] S.H. Lee, J.C. Rasaiah, Molecular dynamics simulation of ion mobility. 2. Alkali metal and halide ions using the SPC/E model for water at 25 °C, J. Phys. Chem. 100 (1996) 1420–1425, http://dx.doi.org/10.1021/jp953050c.
[44] S. Phongphanphanee, N. Yoshida, S. Oiki, F. Hirata, Distinct configurations of cations and water in the selectivity filter of the KcsA potassium channel probed by 3D-RISM theory, J. Mol. Liq. 200 (2014) 52–58, http://dx.doi.org/10.1016/j.molliq.2014.03.050.
[45] C. Ling, J. Chen, F. Mizuno, First-principles study of alkali and alkaline earth ion intercalation in iron hexacyanoferrate: the important role of ionic radius, J. Phys. Chem. C. 117 (2013) 21158–21165, http://dx.doi.org/10.1021/jp4078689.
[46] Y. Moritomo, T. Matsuda, Y. Kurihara, J. Kim, Cubic-rhombohedral structural phase transition in Na 1.32 $Mn[Fe(CN)_6]0.83{\cdot}3.6H_2O$, J. Phys. Soc. Jpn. 80 (2011) 74608, http://dx.doi.org/10.1143/JPSJ.80.074608.
[47] J. Bácskai, K. Martinusz, E. Czirók, G. Inzelt, P.J. Kulesza, M.a. Malik, Polynuclear nickel hexacyanoferrates: monitoring of film growth and hydrated counter-cation flux/storage during redox reactions, J. Electroanal. Chem. 385 (1995) 241–248, http://dx.doi.org/10.1016/0022-0728(94)03788-5.